Available online at www.sciencedirect.com
SCIENCE DIRECT®
ELSEVIER
Journal of Crystal Growth 248 (2003) 186–193
JOURNAL OF CRYSTAL GROWTH
www.elsevier.com/locate/jcrysgro

MOVPE growth of visible vertical-cavity surface-emitting lasers (VCSELs)

M. Zorn*, A. Knigge, U. Zeimer, A. Klein, H. Kissel, M. Weyers, G. Tränkle

Ferdinand-Braun-Institut für Höchstfrequenztechnik, Albert-Einstein-Str. 11, D-12489 Berlin, Germany

Abstract

This paper summarises the development of the epitaxial growth process for visible vertical-cavity surface-emitting lasers (VCSELs) in metal-organic vapour phase epitaxy (MOVPE). The production of these devices which are of particular interest, e.g. for data communications via plastic optical fibres or for consumer electronics, is a real challenge for MOVPE due to the unfavourable material properties in the AlInGaP/AlGaAs material system necessary for this wavelength range. The following stages of the growth process have been investigated with the intention to reach maximum output power and high temperature stability: distributed Bragg reflector (DBR) doping, interface grading, number of p:DBR pairs, oxide confinement layer, cavity design, number of quantum wells, and wavelength alignment. After optimisation devices with record high output powers of more than 4 mW at 650 nm and 10 mW at 670 nm could be fabricated. Single mode VCSELs show laser emission up to 65°C at 650 nm and 87°C at 670 nm. Laser operation for more than 1000 h demonstrates the potential of these devices for industrial applications.
© 2002 Elsevier Science B.V. All rights reserved.

PACS: 81.05.Ea; 81.15.Gh; 42.55.Px; 78.66.Fd

Keywords: A3. Metalorganic vapor phase epitaxy; B2. AlGaAs; B2. AlInGaP; B2. Semiconducting III–V materials; B3. Laser diodes; B3. Vertical cavity surface emitting laser

1. Introduction

Vertical-cavity surface-emitting lasers (VCSELs) [1–3] provide essential advantages as compared to conventional edge emitting lasers. These include a circular beam profile, dynamic single-frequency operation, ease of two-dimensional array fabrication [4] and the possibility of wafer-scale testing. High-performance visible-wavelength VCSELs emitting at a wavelength of 650 nm can be used for technologies like high-density optical storage systems, high-definition laser printing and especially for optical communication systems based on plastic optical fibres which have an absorption minimum at 650 nm. Visible-wavelength VCSELs typically consist of n- and p-doped AlGaAs distributed Bragg reflectors (DBRs) enclosing an AlInGaP cavity containing strained InGaP quantum wells (QWs). With about 200 semiconductor layers the VCSEL structure is very thick ($\approx$8–9 μm). Due to their complexity, these VCSELs raise particular difficulties in the crystal

*Corresponding author. Tel.: +49-30-6392-2676; fax: +49-39-6392-2685.
E-mail address: zorn@fbh-berlin.de (M. Zorn).

0022-0248/03/$ - see front matter © 2002 Elsevier Science B.V. All rights reserved.
PII: S0022-0248(02)01860-2

growth by metal-organic vapour phase epitaxy (MOVPE) [5]. Maintaining tight control of the layer thickness over the long process time is important, and therefore optical techniques have been used for in situ investigations during the growth process. These techniques include single wavelength pyrometry [6,7], reflectance measurements [8–12], spectroscopic ellipsometry [13] as well as reflectance anisotropy spectroscopy (RAS) [11].

The development of red VCSELs started in the early 1990s mainly driven by K.D. Choquette et al. at Sandia National Laboratories (see e.g. Ref. [3]). In the last few years the research was continued in Europe within the BREDSELS project [14,15], at Technical University of Stuttgart [16] and at FBH Berlin [11,17] using MOVPE and at Tampere University of Technology also via solid-source MBE [18].

In this paper, the development of the epitaxial VCSEL structure is reported with the aim of reaching maximum output power and high temperature stability for 650–670 nm devices. The focus is on the crucial constituents of the VCSEL device: the DBR mirror and the cavity. Therefore, in the first part the DBR design is investigated while in the second part the cavity design is the centre of interest.

2. Experimental procedure

All epitaxial layer structures presented in this work were grown in Aixtron 200 and 200/4 low-pressure MOVPE systems. The sources used are trimethylgallium (TMGa), triethylgallium (TEGa), trimethylaluminum (TMAl), trimethylindium (TMIn), arsine (AsH_3) and phosphine (PH_3). Silicon (Si) from Si_2H_6 was used for n-doping. Zinc (Zn) from dimethylzinc (DMZn) and intrinsically incorporated carbon (C) were utilised for p-doping. The growth pressure was 100 and 150 mbar and a typical growth temperature was 770°C. Epiready n^+ GaAs (1 0 0) substrates misoriented 6° towards [1 1 1] A were used.

The MOVPE systems are equipped with low-strain UV transparent viewports for normal incidence optical access and with a corresponding hole in the liner-tube. In situ measurements were performed using a LayTec EpiRAS-200 spectrometer that allows combined RAS [19,20] and reflectance (R) measurements under standard device growth conditions [21].

The layer structures were processed into air-post/oxide confined mesa-type VCSELs of 30–60 μm diameter which were characterised for their device properties under pulsed and continuous-wave (cw) excitation [22].

3. Results and discussion

3.1. Structure and characterisation

Fig. 1a shows a sketch of a typical VCSEL structure emitting visible red light. It consists of a n-doped bottom DBR with 55.5 pairs of $Al_{0.50}Ga_{0.50}As/AlAs$ and a cavity with three InGaP quantum wells embedded in AlInGaP. The p-doped top DBR consists of 35 pairs of $Al_{0.50}Ga_{0.50}As/Al_{0.95}Ga_{0.05}As$ except for the third pair being $Al_{0.50}Ga_{0.50}As/Al_{0.98}Ga_{0.02}As$ in order to facilitate the formation of an aperture by wet oxidation.

The growth of the VCSEL structures was monitored in situ. Fig. 1(b) shows the development of the normalised reflectance R/R_{GaAs} [11] at 704 nm (1.76 eV) which is near the reflectance stop band centre at growth temperature. A strong increase in reflectance can be seen during the growth of the first ten mirror pairs together with a following saturation. After growth of the AlInGaP cavity a strong decrease in reflectance occurs due to the resonance effect in the cavity. With increasing number of p:DBR pairs the reflectance increases again and saturates at the end of the growth process. Besides, in situ spectral reflectance measurements have been shown to be essential for the alignment of the n- and p-DBR and therefore for the final device properties [11]. Fig. 1(c) shows a reflectance anisotropy (RA) transient taken at 310 nm (4.00 eV). Since RAS was shown to be sensitive to the doping type and concentration [11,23], the different doping levels of the n- and p-DBR can be distinguished by the different RA signal. In this particular case, the growth of the

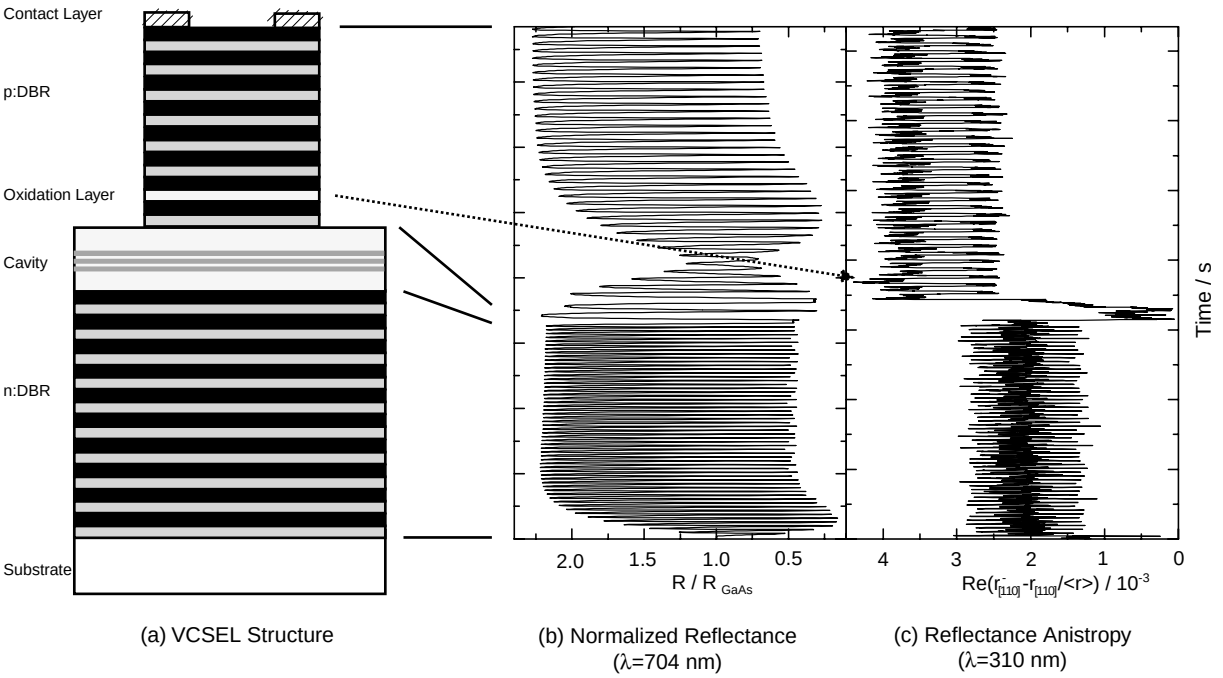

Fig. 1. (a) Sketch of a VCSEL structure emitting at a wavelength around 650 nm. (b) Transient of the normalised reflectance R/R_{GaAs} at 704 nm (1.76 eV) taken during growth. (c) Transient of the reflectance anisotropy taken during growth at 310 nm (4.00 eV).

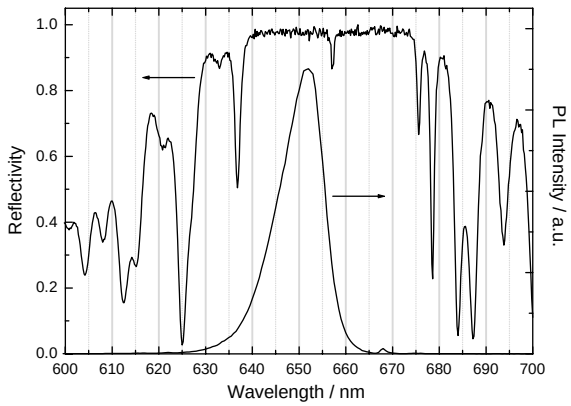

Fig. 2. Reflectance spectrum (left axis) of a complete VCSEL structure after removing the GaAs contact layer and photoluminescence spectrum (right axis) after removing the p:DBR.

oxide confinement layer can also be resolved by a peak in the RA signal.

A typical ex-situ spectral reflectance spectrum taken after removing the GaAs contact layer by wet etching is shown in Fig. 2 (left axis). The typical high reflectance stop band arises together with the sharp reflectance dip near 650 nm caused by the cavity resonance. In contrast to reflectance spectra taken on the complete structure [11], these spectra are not affected by the absorption in the contact layer and therefore show a reflectivity near one. The room temperature PL spectrum of the active region (right axis) was measured with the p-DBR removed to avoid its filtering effect. It can be seen that there is a detuning between the cavity resonance and QW wavelength. In this particular case, the QW emission is about 5 nm shorter than the cavity resonance. This detuning can be used to improve the thermal stability of VCSEL devices as shown below.

3.2. DBR design

Since the DBR mirrors consist of 110 n-DBR and 70 p-DBR layers to achieve the very high

reflectance, the DBRs have a strong influence on the series resistance of the final device.

We investigated the influence of different doping elements and interface grading in the p:DBR on the resistance. The p:DBR was chosen, since its influence is higher due to the reduced hole mobility. The series resistance decreases when changing the p-dopant from Zn to C [24]. This might be explained by the fact that for Zn doping all layers have the same doping concentration, while in the C-doped layers the doping concentration in the AlAs layers is increased in contrast to the $Al_{0.50}Ga_{0.50}As$ layers where the doping concentration is reduced [22]. While an increase in the doping level reduces the series resistance it can also lead to higher threshold current densities due to increased absorption [22]. Here a compromise has to be found. Introducing graded interfaces leads to a further decrease in the series resistance [24].

The reflectance of the DBR mirrors increases with increasing number of DBR pairs. The n:DBR consists of 55.5 DBR pairs to ensure maximal reflectivity. The reflectivity of the p:DBR must be high enough for laser operation but lower than the n:DBR reflectivity to assure light emission via the top DBR. Fig. 3 shows the dependence of the threshold current density j_{th} and pulsed output power in dependence on the number of p:DBR pairs while keeping the number of n:DBR layers constant. It can be seen, that with increasing number of p:DBR pairs j_{th} decreases due to the increasing reflectance which eases laser operation. However, this increase in reflectance leads to a decrease in output power for more than 35 p:DBR pairs. The decrease in output power for less than 35 p:DBR pairs can be explained by thermal losses caused by an increasing j_{th}.

Devices with etched mesa structures show laser operation in pulsed mode only. CW operation of VCSELs can be achieved by introducing an aperture into the mesas. This can be done either by ion implantation [25,26] or wet oxidation of the AlGaAs layers with a very high aluminium content [27]. The necessary low gallium concentrations are difficult to achieve using normal mass flow controller (MFC) configurations in conjunction with the common precursors TMGa and TMAl. Therefore, we used TEGa as Ga source which has a much lower vapour pressure than TMGa. Fig. 4 shows a SEM picture of a mesa with an aperture created by wet oxidation. The sharp oxidation front of the AlGaAs layers with $x = 0.95$ can clearly be seen. The oxidation rate for $x = 0.98$ is about 3 times higher which leads to the deeper oxidation of the 5th layer of the p:DBR. Furthermore, it was also shown that it is essential to add small amounts of Ga ($\geqslant 2\%$) instead of using pure AlAs to achieve stable oxidised DBR mirrors [28].

The diameter of the resulting aperture has a strong influence on the final device properties as

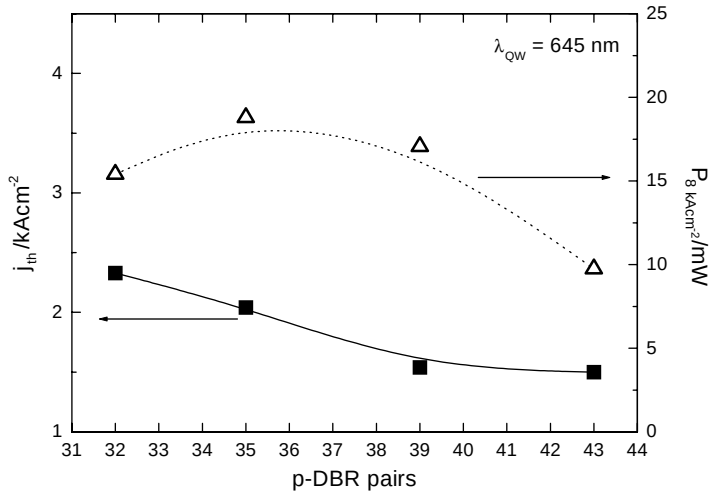

Fig. 3. Dependence of threshold current density (left axis) and pulsed output power (right axis) on p:DBR pair number.

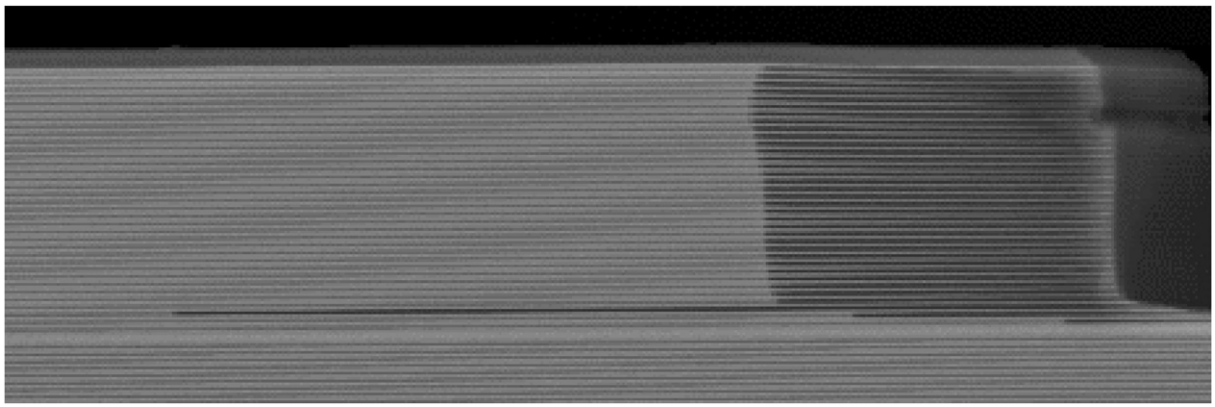

Fig. 4. SEM micrograph of the edge of a VCSEL mesa showing the oxide aperture layer.

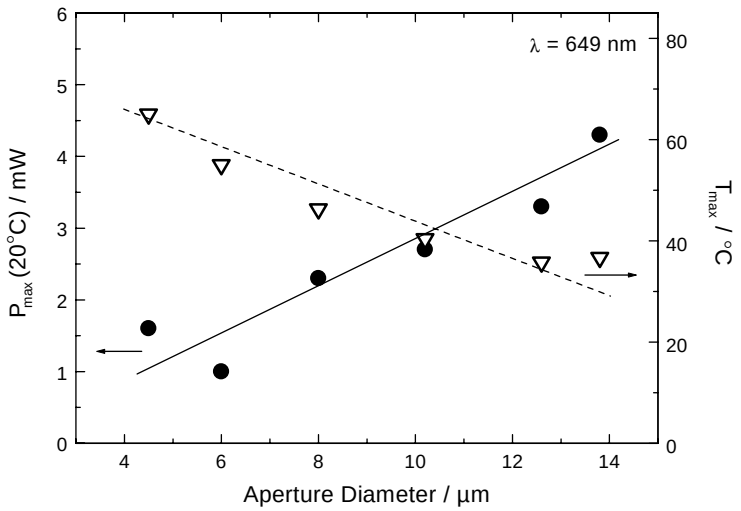

Fig. 5. Dependence of maximum cw output power (left axis) and maximum operation temperature (right axis) on aperture size.

can be seen in Fig. 5. The left axis shows the dependence of cw output power on aperture diameter. For small diameters of about 4 µm the output power is around 1 mW and increases strongly to more than 4 mW for 14 µm diameter. In contrast, the maximal operation temperature for laser operation (right axis), which is limited by leakage over the low barriers in the conduction band in the active region, decreases from 65°C to 35°C. This demonstrates the strong influence of the aperture size together with the need for a high reproducibility of the wet oxidation process for a tight control of the diameter.

Table 1
Comparison of different cavity designs

	j_{th} (650 nm)	$P_{pulsed,\ 8\ kA/cm^2}$ (650 nm)
Without spacer	5.4 kA/cm^2	10.0 mW
With spacer	2.3 kA/cm^2	18.0 mW

3.3. Cavity design

The cavity consists of three InGaP QWs embedded in $(Al_{0.50}Ga_{0.50})_{0.52}In_{0.48}P$. To reduce the influence of the leakage current known to be one of the main problems for these short

wavelength devices [29,30], we introduced an $(Al_{0.67}Ga_{0.33})_{0.52}In_{0.48}P$ spacer layer on both sides of the cavity. In Table 1 the resulting threshold current densities are compared for the different structures at an emission wavelength of 650 nm. The additional spacer layers lead to a reduction of the threshold current density from 5.4 to 2.3 kA/cm^2. A strong increase in output power can also be obtained. The pulsed output power nearly doubles from 10 to 18 mW at 650 nm at a constant current density of 8 kA/cm^2. This can be explained by enhanced carrier confinement in the QWs leading to reduced carrier leakage [31].

Furthermore we investigated the influence of the QW number. Fig. 6 shows the dependence of j_{th} and pulsed output power at 8 kA/cm^2 for structures with three, four and five QWs. It can be seen that there is a slight decrease in j_{th} when increasing the number of QWs from three to four and a strong increase at five QWs. The output power has a maximum at four QWs.

Fig. 7 shows the dependence of j_{th} and pulsed output power on the QW-cavity detuning (as defined in Fig. 2). It can be seen that j_{th} has a minimum when the QW wavelength is shorter than the cavity resonance wavelength. On the other hand, the maximal output power can be achieved when the QW wavelength is tuned slightly longer than the cavity resonance. Summarising, this shows that for red VCSELs only a small detuning is needed for best device properties. This is in agreement with results reported in Ref. [16] where best results could be achieved for a QW-cavity detuning of −1 nm.

3.4. Further developments

For contacting the devices, the growth process ends with a highly p-doped GaAs contact layer of 84 nm thickness [11]. Unfortunately, GaAs is absorbing at wavelengths below 870 nm. Therefore, a further enhancement can be achieved by removing the contact layer from the final device. To control this process an additional p-$In_{0.48}Ga_{0.52}P$ etch stop layer is introduced at the end of the last p-DBR layer, which is also necessary to prevent the top AlGaAs layer from oxidation. Table 2 shows the difference in j_{th} and cw output power when the GaAs contact layer is removed. Beside a small reduction of j_{th} the main effect is the increase in output power by a factor of 2.5.

All those improvement steps resulted in devices with record high output powers of more than 4 mW at 650 nm and 10 mW at 670 nm [32]. Single mode VCSELs show laser emission up to 65°C at 650 nm and 87°C at 670 nm.

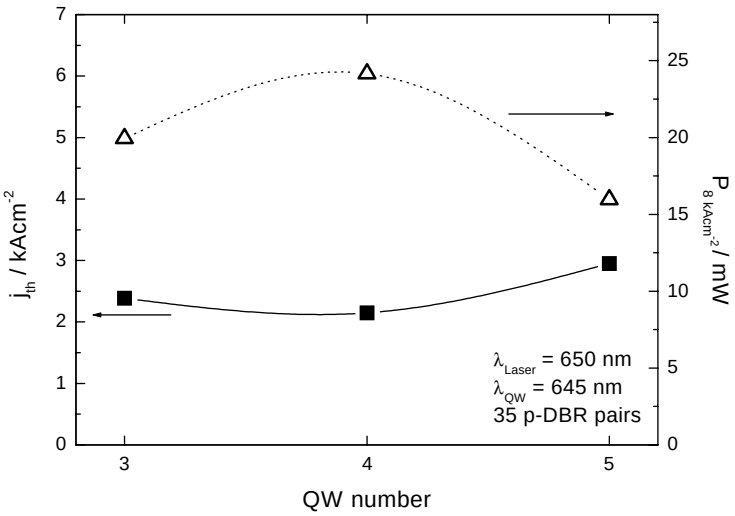

Fig. 6. Dependence of threshold current density (left axis) and pulsed output power (right axis) on QW number.

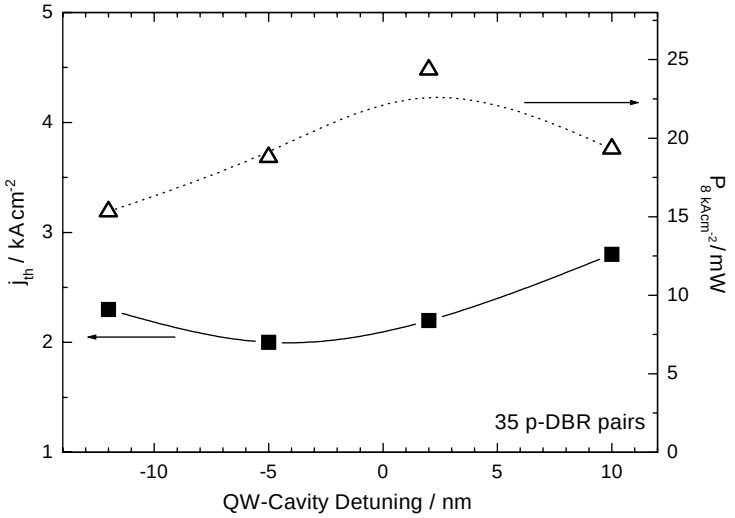

Fig. 7. Dependence of threshold current density (left axis) and pulsed output power (right axis) on QW-cavity detuning.

Table 2
Comparison of VCSEL devices with and without contact layer

	j_{th} (650 nm)	P_{cw} (650 nm)
With contact layer	2.1 kA/cm^2	1.3 mW
Without contact layer	1.7 kA/cm^2	3.2 mW

Reliability tests show laser operation over 1000 h at 20°C ($P = 0.4$ mW) and at 40°C ($P = 0.1$ mW) [33].

4. Summary

The development of the epitaxial growth process for red vertical-cavity surface-emitting lasers is reviewed. The investigations show that the optimum structure consists of 35 p:DBR pairs and four QWs. Furthermore, the output power and the thermal stability can be increased by introducing additional spacer layers. Finally, removing the GaAs contact layer leads to record high output powers of more than 4 mW at 650 nm and 10 mW at 670 nm. Single mode VCSELs show laser emission up to 65°C at 650 nm and 87°C at 670 nm. Laser operation could be shown for more than 1000 h at 40°C.

Acknowledgements

Support for this work by the Deutsche Forschungsgemeinschaft (DFG) under contract TR357-1/2 is acknowledged. The authors like to thank O. Fink for the assistance at the MOVPE systems, H. Wenzel for device modelling and the colleagues of FBH's process technology department for the device processing.

References

[1] C. Wilmsen, H. Temkin, L.A. Coldren, Vertical-Cavity Surface-Emitting Lasers, Design, Fabrication, Characterization, and Applications, Cambridge University Press, Cambridge, 1999.
[2] T.E. Sale, Vertical Cavity Surface Emitting Lasers, Research Studies Press Ltd., Taunton, 1995.
[3] W.W. Chow, K.D. Choquette, M.H. Crawford, K.L. Lear, G.R. Hadley, IEEE J. Quant. Electron. 33 (1997) 1810.
[4] B. Corbett, T. Calvert, J.D. Lambkin, Electron. Lett. 36 (2000) 1464.
[5] R.P. Schneider Jr., R.P. Bryan, J.A. Lott, E.D. Jones, G.R. Olbright, J. Crystal Growth 124 (1992) 763.
[6] G. Böhm, M. Hauser, M. Sexl, G. Tränkle, G. Weimann, G. Abstreiter, Proc. SPIE 3286 (1998) 113.
[7] Y.M. Houng, M.R.T. Tan, B.W. Liang, S.Y. Wang, D.E. Mars, J. Vac. Sci. Technol. B 12 (1994) 1221.
[8] K.P. Killeen, W.G. Breiland, J. Electron. Mater. 23 (1994) 179.

[9] W.G. Breiland, H.Q. Hou, H.C. Chui, B.E. Hammons, J. Crystal Growth 174 (1997) 564.
[10] F. Van Dijk, V. Bardinal, C. Fontaine, E. Bedel-Pereira, A. Muñoz-Yagüe, J. Crystal Growth 201/202 (1999) 1028.
[11] M. Zorn, K. Haberland, A. Knigge, A. Bhattacharya, M. Weyers, J.-T. Zettler, W. Richter, J. Crystal Growth 235 (2002) 25.
[12] K. Haberland, M. Zorn, M. Klein, A. Bhattacharya, M. Weyers, J.-T. Zettler, W. Richter, J. Crystal Growth 248 (2003) 194–200.
[13] G.N. Maracas, J.L. Edwards, D.S. Gerber, R. Droopad, Appl. Surf. Sci. 63 (1993) 1.
[14] J.D. Lambkin, T. Calvert, B. Corbett, J. Woodhead, S.M. Pinches, A. Onischenko, T.E. Sale, J. Hosea, P. Van Dale, K. Van De Putte, A. Van Hove, V. Adriaan, J.G. McInerney, P.A. Porta, Proc. SPIE 3946 (2000) 95.
[15] T. Calvert, B. Corbett, J.D. Lambkin, Electron. Lett. 38 (2002) 222.
[16] R. Butendeich, D. Graef, J. Schwarz, T. Ballmann, H. Schweizer, F. Scholz, J. Crystal Growth 221 (2000) 657.
[17] A. Knigge, M. Zorn, H. Wenzel, M. Weyers, G. Tränkle, Electron. Lett. 37 (2001) 1222.
[18] M. Saarinen, M. Toivonen, N. Xiang, V. Vilokkinen, M. Pessa, Electron. Lett. 36 (2000) 1210.
[19] D.E. Aspnes, Mater. Sci. Eng. B 30 (1995) 109.
[20] J.-T. Zettler, K. Haberland, M. Zorn, M. Pristovsek, W. Richter, P. Kurpas, M. Weyers, J. Crystal Growth 195 (1998) 151.
[21] K. Haberland, P. Kurpas, M. Pristovsek, J.-T. Zettler, M. Weyers, W. Richter, Appl. Phys. A 68 (1999) 309.
[22] A. Oster, M. Zorn, K. Vogel, J. Fricke, J. Sebastian, W. John, M. Weyers, G. Tränkle, Proc. SPIE 4286 (2001) 148.
[23] M. Pristovsek, S. Tsukamoto, N. Koguchi, B. Han, K. Haberland, J.-T. Zettler, W. Richter, M. Zorn, M. Weyers, Phys. Status Solidi A 188 (2001) 1423.
[24] A. Bhattacharya, M. Zorn, A. Oster, M. Nasarek, H. Wenzel, J. Sebastian, M. Weyers, G. Tränkle, J. Crystal Growth 221 (2000) 663.
[25] X.M. Li, Y.C. Chang, J.F. Song, Y.S. Zhao, G.T. Du, J.A. Lott, R.P.H. Chang, Opt. Quant. Eletron. 31 (1999) 303.
[26] K. Takaoka, M. Ishikawa, G. Hatakoshi, IEEE J. Sel. Top. Quantum Electron. 7 (2001) 381.
[27] D.L. Huffaker, D.G. Deppe, K. Kumar, T.J. Rogers, Appl. Phys. Lett. 65 (1994) 97.
[28] K.D. Choquette, K.M. Geib, H.C. Chui, B.E. Hammons, H.Q. Hou, T.J. Drummond, Appl. Phys. Lett. 69 (1996) 1385.
[29] W.W. Chow, M.H. Crawford, R.P. Schneider Jr., IEEE J. Sel. Top. Quantum Electron. 1 (1995) 649.
[30] G. Knowles, S.J. Sweeney, T. Sale, IEE Proc. Optoelectron. 148 (2001) 55.
[31] A. Knigge, M. Zorn, J. Sebastian, K. Vogel, H. Wenzel, M. Weyers, G. Tränkle, IEE Proc. Optoelectron., in print.
[32] A. Knigge, M. Zorn, M. Weyers, Electron. Lett. 38 (2002) 882.
[33] A. Knigge, R. Franke, S. Knigge, B. Sumpf, K. Vogel, M. Zorn, M. Weyers, G. Tränkle, Photon. Technol. Lett., in print.